AGU PUBLICATIONS

Geophysical Research Letters

RESEARCH LETTER
10.1002/2014GL060100

Key Points:
- Hiss intensity model is developed as a function of *Kp*, *L*, and latitude
- Electron lifetimes are strongly dependent on *Kp*, MLT, energy, and distance
- We provide coefficients for models of hiss intensity and electron lifetimes

Supporting Information:
- Readme
- Table S1
- Table S2
- Table S3
- Table S4
- Text S1

Correspondence to:
K. Orlova,
ks13orl@gmail.com

Citation:
Orlova, K., M. Spasojevic, and Y. Shprits (2014), Activity-dependent global model of electron loss inside the plasmasphere, *Geophys. Res. Lett.*, *41*, doi:10.1002/2014GL060100.

Received 15 APR 2014
Accepted 24 MAY 2014
Accepted article online 27 MAY 2014

Activity-dependent global model of electron loss inside the plasmasphere

Ksenia Orlova[1,2], Maria Spasojevic[3], and Yuri Shprits[4,1]

[1]Department of Earth, Planetary, and Space Sciences, University of California, Los Angeles, California, USA, [2]Skobeltsyn Institute of Nuclear Physics, Lomonosov Moscow State University, Moscow, Russia, [3]Department of Electrical Engineering, Stanford University, Stanford, California, USA, [4]Department of Earth, Atmospheric, and Planetary Sciences, Massachusetts Institute of Technology, Cambridge, Massachusetts, USA

Abstract Using data from the CRRES plasma wave experiment, we develop quadratic fits to the mean of the wave amplitude squared for plasmaspheric hiss as a function of *Kp*, *L*, and magnetic latitude (λ) for the dayside ($6 <$ magnetic local time (MLT) ≤ 21) and nightside ($21 <$ MLT ≤ 6) magnetic local time sectors. The empirical model of hiss waves is used to compute quasi-linear pitch angle diffusion coefficients for energetic, relativistic, and ultrarelativistic electrons in the energy range of 1 keV to 10 MeV. In our calculations, we account for changes in hiss wave normal angle and plasma density with increasing λ. Electron lifetimes are then calculated from the diffusion coefficients and parameterized as a function of energy, *Kp*, and *L*. Coefficients for both the hiss model and the electron lifetimes are provided and can be easily incorporated into existing diffusion, convection, and particle tracing codes.

1. Introduction

Plasmaspheric hiss is a whistler mode emission that permeates the Earth's plasmasphere and is a significant driver of energetic electron losses through cyclotron-resonant pitch angle scattering [e.g., *Millan and Thorne*, 2007; *Shprits et al.*, 2008, and references therein]. Hiss is believed to be largely responsible for the formation of the slot region between the inner and outer electron belts [e.g., *Lyons et al.*, 1972; *Lyons and Thorne*, 1973; *Abel and Thorne*, 1998; *Meredith et al.*, 2007, 2009] and plays a major role in reducing the flux of relativistic electrons that build up in the aftermath of geomagnetic storms [e.g., *Abel and Thorne*, 1998; *Meredith et al.*, 2006b; *Shprits et al.*, 2009, 2013b; *Thorne et al.*, 2013]. Therefore, accurate quantification of electron lifetimes due to scattering by hiss is a critical component to modeling and predicting the global dynamics of the electron radiation belts.

Maps of plasmaspheric hiss wave intensity from the CRRES mission were first presented by *Meredith et al.* [2004] and have been used in a number of studies examining the origin of the waves [*Meredith et al.*, 2006a; *Bortnik et al.*, 2008] as well as their effect on energetic electron lifetimes [e.g., *Meredith et al.*, 2006b, 2007; *Summers et al.*, 2008; *Lam et al.*, 2009; *Meredith et al.*, 2009]. Here we independently derive a database of hiss observations from the CRRES plasma wave experiment using a nearly identical procedure to *Meredith et al.* [2004] and develop analytical quadratic models for the time-averaged hiss magnetic field intensity $<B_w^2>$ as a function of *Kp*, *L*, and λ for two local time sectors.

The effect of hiss waves on energetic electron lifetimes has been explored observationally by analyzing the decay rates of fluxes from various satellites for both the slot region and the outer radiation belt [e.g., *Baker et al.*, 1994; *Meredith et al.*, 2006b, 2007, 2009; *Benck et al.*, 2010]. Loss time scales are usually calculated using diffusion theory and are in reasonable agreement with the decay rates obtained from observations [e.g., *Abel and Thorne*, 1998; *Albert*, 2000; *Selesnick et al.*, 2003; *Meredith et al.*, 2006b, 2007, 2009]. Most recently, *Mourenas and Ripoll* [2012] and *Artemyev et al.* [2013] have developed a formalism that allows them to analytically estimate electron lifetimes.

Abel and Thorne [1998] calculated electron lifetimes for energies 100, 300, 500, 900, and 1500 keV. They accounted for Coulomb scattering and scattering by whistler waves at distances up to $L = 4$. Their results indicated that the outer radiation belt lifetimes due to hiss waves range from several days to over a hundred days. *Meredith et al.* [2006b] computed lifetimes for electron energies of 214 keV, 510 keV, and 1.09 MeV for $Kp < 3$ and showed that their results were similar to the observed decay rates. *Summers et al.* [2008] calculated

electron lifetimes by hiss waves in plasmaspheric plumes at distances $L = 3.5–7$ for energies of 100, 200, 500, and 1000 keV using realistic hiss wave amplitudes and plasma density from CRRES. Their results showed that lifetimes for electrons of a few hundred keV were about 1 day or less, and for larger energies, the typical lifetimes became several days. *Chen and Schulz* [2001] developed a model of losses for diffuse auroral particles that accounted for strong diffusion in the outer region and provided a smooth transition to slower loss in the inner magnetosphere. Thus, in the previous theoretical studies, lifetimes were computed at specific energies and usually for 2 or 3 ranges of the *Kp* or AE^* indices. In this study, we present a comprehensive model of lifetimes in the outer radiation belt due to resonant hiss-electron interaction as a continuous function of electron energy, distance, and *Kp* index. We calculate loss time scales using realistic hiss amplitudes and plasma parameters and compare the calculated lifetimes with previous observational studies. In addition, both the empirical hiss model and the computed lifetimes are parameterized using simple analytical functions and thus can be widely used in 2-D, 3-D, and 4-D convection and particle tracing codes.

2. Empirical Model of Plasmaspheric Hiss Intensity

The sweep frequency receiver (SFR) on the CRRES plasma wave experiment provides wave measurements from 100 Hz to 400 kHz in 128 log-spaced frequency bins from a single 100 m tip-to-tip electric dipole antenna oriented perpendicular to the spacecraft spin axis, which was in the ecliptic plane [*Anderson et al*., 1992]. Our analysis uses SFR measurements of electric (*E*) field power spectral density (PSD) from 19 August 1990 to 12 October 1991 (orbits 61–1067). Plasmaspheric hiss is defined as wave power in the frequency range of 100 Hz to 2 kHz that lies inside the plasmapause or within regions of high-density "detached" plasma, such as plasmaspheric plumes. We use a database of plasmapause crosses derived from the CRRES SFR data provided by *Moldwin et al*. [2002]. For passes where no plasmapause is identified (e.g., shallow density gradients) and to identify detached plasma regions, we examine the relative intensity of electrostatic electron cyclotron harmonic waves (high-density regions are generally devoid of electron cyclotron harmonic waves), such as was done by *Meredith et al*. [2004].

To calculate hiss wave intensity, we first remove data spikes and apply a frequency-dependent background subtraction provided by *Meredith et al*. [2004]. Next, we compute 3 min running averages of the PSD to remove the effects of the spinning spacecraft and multiply by a factor of 2 to estimate the total PSD in the spin plane. Then, we convert the *E*-field PSD to magnetic (*B*) field PSD using the parallel propagating whistler mode dispersion relationship [see *Meredith et al*., 2004, equation (1)] along with measurements of the local background magnetic field and estimates of the cold plasma density derived from the upper hybrid resonance line observed in the higher frequency bands of the SFR [*LeDocq et al*., 1994]. As was discussed by *Meredith et al*. [2004], the assumption of parallel propagation is justified since in the hiss frequency band and for typical values of the plasma-to-gyrofrequency ratio, the conversion of *E* to *B* is relatively insensitive to wave normal for angles $<50°$. Next, the *B*-field PSD is integrated from 100 Hz to 2 kHz to yield the hiss wave intensity, B_w^2.

In order to develop an empirical model of the average hiss wave intensity, we divide the data into two local time sectors, $6 < \mathrm{MLT} \le 21$ (dayside) and $21 < \mathrm{MLT} \le 6$ (nightside) and limit the data to regions of highest coverage, $3 \le L \le 6$ and $|\lambda| \le 25°$. The value of *Kp* is linearly interpolated to each data point. There are a total of 359,276 dayside and 258,868 nightside hiss measurements. For each local time sector, we divide the data into 10% quantile bins in *Kp*, *L*, and λ and compute the average value of B_w^2 in this $10 \times 10 \times 10$ grid. The averages as a function of λ and *L* can be seen for three ranges of *Kp* for the dayside in Figures 1a–1c and for nightside in Figures 1g–1i. We note that binning and averaging the data prior to performing the regression analysis are critical steps in creating a wave model appropriate for use in calculating diffusion coefficients. Performing regression on the full data set prior to averaging will result in an empirical model of the *median* wave intensity, which can be an order of magnitude smaller than the mean and is not the appropriate quantity for calculating wave driven diffusion.

Next, we use stepwise linear regression to fit the logarithm of $<B_w^2>$ to a polynomial of order up to two (including interaction terms) of the form

$$\log_{10}\left(< B_w^2 >\right) = w_0 + w_1 Kp + w_2 L + w_3 \lambda + w_4 Kp\lambda + w_5 L\lambda + w_6 Kp^2 + w_7 L^2 + w_8 \lambda^2, \quad (1)$$

where the weights of the model w_n are provided in Table 1. We apply a stepwise fitting technique in

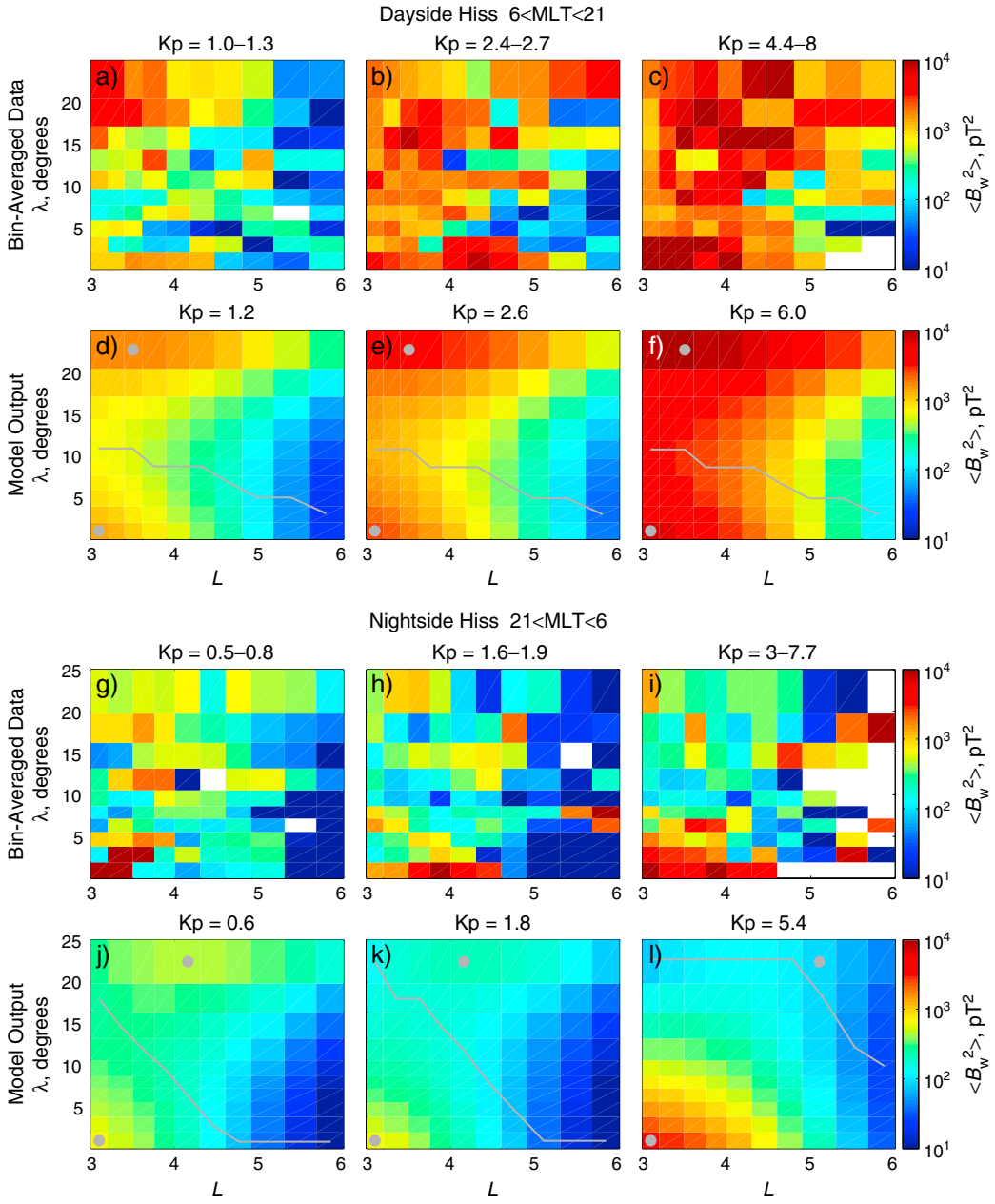

Figure 1. Bin-averaged values of B_w^2 as a function of λ and L for three ranges of the Kp index are shown for (a–c) dayside hiss and for (g–i) nightside hiss. Output of the quadratic model for three values of Kp for (d–f) dayside hiss and (j–l) nightside hiss. The gray lines overlaid on the model output indicate the λ of the minimum hiss intensity as a function of L, and the gray dots indicate the two local maxima.

which weights for the full model are first estimated, and terms are successively removed if they do not contribute to the model in a statistically significant way (e.g., there is no KpL term for either model and the $Kp\lambda$ term is removed on the dayside). We note that all values of Kp are included in the bin-averaged data, but due to sparse data at high Kp, the model is only considered valid for $Kp \leq 6$. Also, the model is only valid

Table 1. Table of Weights for the Quadratic Model of Hiss Intensity Described by Equation (1)

Model	w_0	w_1	w_2	w_3	w_4	w_5	w_6	w_7	w_8
Dayside	2.559	0.2607	0.5555	−0.1263	0	0.01815	−0.01547	−0.1400	0.003092
Nightside	2.432	−0.08824	0.6392	−0.1361	−0.01267	0.03026	0.04248	−0.1569	0.001457

when the region of interest is inside the plasmasphere or plasmaspheric plume and should be used in conjunction with a plasmapause model. The coefficient of determination, R^2, is a measure of goodness of fit for regression models and is interpreted as the percentage of variation in the bin-averaged data that can be explained by the model. The value of R^2 is 0.51 for the dayside model and 0.28 for the nightside model. For this particular application, the absolute value of R^2 is largely dependent on the number of bins used in the calculation of $<B_w{}^2>$. For example, using fewer bins results in smoother bin-averaged data values, which in turn are easier to fit with the quadratic model and improves the value of R^2. However, for any level of binning, the nightside model has a lower value of R^2 than the dayside model. Overall, the data on the nightside have a higher degree of variance. The variance could be captured with a higher order model, but this runs the risk of overfitting. The root-mean-square error (RMSE) is a measure of accuracy for a regression model and represents the standard deviation of the error between the bin-averaged data and the model prediction. The RMSE has the same units as the model output, $\log_{10}(pT^2)$, and is 0.53 for the dayside model and 0.79 for the nightside model. In a manner similar to R^2, decreasing the number of bins in the averaging reduces the RMSE, and the nightside model has a higher RMSE regardless of binning.

The output of the quadratic model for the three values of *Kp* are shown in Figures 1d–1f for the dayside hiss and in Figures 1j–1l for the nightside hiss. On the dayside for $L < 4.5$, the hiss intensity as a function of λ exhibits a minimum near 10° (gray curve) with higher intensities near the equator and above 20°. For $L > 4.5$, the latitude of minimum hiss intensity moves toward the equator, and hiss intensity generally increases with increasing λ. These trends continue across all levels of activity. Overall, the hiss intensity is significantly weaker on the nightside than on the dayside. On the nightside for low activity (Figure 1j), the hiss intensity peaks near the equator for $L < 3.5$ but is more intense at higher λ for $L > 3.5$. With increasing *Kp*, the hiss intensifies near the equator and decreases at higher λ.

3. Lifetimes of Electrons

3.1. Hiss Wave Model

To calculate the electron lifetimes due to hiss, we start with the hiss intensity dependencies from equation (1), which are valid for latitudes less than 25°. Since the past work has shown that hiss can extend up to ~45° in latitude and is still rather strong at latitudes larger than 25° [e.g., *Agapitov et al*., 2013], we assume that for latitudes from 25° to 45° hiss, amplitudes are the same as for 25° latitude. Following previous studies [e.g., *Shprits et al*., 2009; *Thorne et al*., 2013], the frequency spectrum of hiss is modeled as Gaussian with the maximum frequency $f_m = 550$ Hz, bandwidth $\delta f = 300$ Hz, and lower and upper cutoffs $f_{lc} = 100$ Hz and $f_{uc} = 2000$ Hz, respectively. The wave normal angle distribution is taken as a latitudinal dependent Gaussian with parameters taken from Table S3 in the supporting information of *Thorne et al*. [2013], which were consistent with the observations of *Agapitov et al*. [2013]. Hiss waves become more oblique with increasing latitude, and therefore, the wave normal angles may reach the resonance cone. Since we use the cold plasma theory in the present study, we cut off the wave normal angles near the resonance cone.

3.2. Calculation of Lifetimes

Electron lifetime, τ, is computed using an integral expression from *Albert and Shprits* [2009]

$$\tau = \int_{\alpha_{lc}}^{\pi/2} d\alpha_{eq} \left(2 < D_{\alpha\alpha} > \tan(\alpha_{eq})\right)^{-1}, \quad (2)$$

where α_{eq} is the equatorial pitch angle and α_{lc} is the equatorial loss cone angle. $<D_{\alpha\alpha}>$ is the bounce-averaged pitch angle diffusion coefficient calculated in the dipole field model using a quasi-linear approach of *Glauert and Horne* [2005]. The scattering rates are also MLT-averaged proportional to the MLT sectors, where hiss waves are present; that is, the calculated diffusion coefficients are multiplied by 15/24 and 9/24 for the dayside and nightside models, respectively. It follows from equation (2) that electron lifetimes are mainly determined by the minimum value of $<D_{\alpha\alpha}>\tan\alpha_{eq}$. For electrons of tens to hundreds of keV, this minimum occurs at middle equatorial pitch angles, where the scattering rates have a deep local minimum. The exact location of the minimum depends on the *L* shell of interest and energy. For electrons of relativistic energy, the minimum value of $<D_{\alpha\alpha}>\tan\alpha_{eq}$ is reached near the loss cone. Our sensitivity tests show that for $E_k \sim 1$ MeV at $L = 3.5$, the dominant scattering occurs at latitudes of approximately 25°. With increasing distance or energy, the resonant hiss-electron interaction near the loss cone occurs at higher latitudes. Thus, for energies

larger than approximately 0.1–1 MeV (slightly smaller energies for larger distances), the lifetimes are mostly determined by the extent of the hiss waves in latitude. The model of the latitudinal distribution is discussed in section 3.1. Since hiss wave amplitudes are not well known at high latitudes larger than ~25°, better knowledge on latitudinal distribution of hiss waves will help us to improve the model of lifetimes at relativistic energies in the future.

With increasing energy, a larger number of resonances contributes to the scattering rates [e.g., *Mourenas and Ripoll*, 2012]. For example, for relativistic energies above 1 MeV, more than ±5 resonances should be taken into account. Thus, we compute the diffusion coefficients up to $\pm N_r$ resonances dependent on electron energy including Landau resonance. Following *Mourenas and Ripoll* [2012], we define the number of significantly contributing resonances, N_r, as

$$N_r = \left\lceil p\left(2\pi f_m \omega_{pe}^2/\Omega_c^3\right)^{1/2} \sin\vartheta_{\max} \right\rceil, \tag{3}$$

where the brackets represent the ceiling function, p is the dimensionless momentum of the electrons (i.e., momentum divided by the electron mass and the speed of light), ω_{pe} is the plasma frequency, Ω_c is the electron gyrofrequency, and $\theta_{\max} = 85°$ is the maximum wave normal angle. Since with increasing latitude, the number of resonances N_r decreases, we compute it using the equatorial values of ω_{pe} and Ω_c.

Plasmaspheric density n is calculated using the expressions of *Denton et al.* [2004, 2006] for the equatorial density n_{eq} and the increase of density with increasing latitude

$$\log_{10} n_{eq} = -0.324L + 3.78 + [0.00127\, R_{\text{Sun}} - 0.0635]\, e^{(2-L)/1.5}, \tag{4}$$

$$n = n_{eq}(\cos\lambda)^{-2}, \tag{5}$$

where R_{Sun} is the average sunspot number and is assumed to be 78, which is the average value between the solar maximum and minimum values.

Figure 2 shows calculated lifetimes of electrons with energies from 1 keV to 10 MeV for the dayside (top row) and nightside (bottom row) for various levels of geomagnetic activity. Lifetimes are calculated for the same L shells (3–6) and Kp values (0–6) for which the hiss wave intensity model (equation (1)) is valid. The dark red color in Figure 2 corresponds to the regions, where lifetimes of electrons are larger than 1000 days. On the dayside, the lifetimes are several times smaller than those on the nightside. Therefore, electron lifetimes in 21–6 MLT sector due to scattering by hiss can generally be neglected.

On the dayside, lifetimes become significantly shorter with increasing geomagnetic activity (Figures 2a–2d). For example, for 158 keV electrons at $L = 4.5$, lifetimes for $Kp = 0.75$, 3, and 6 are 2.75 days, 1 day, and 10 h, respectively. On the nightside, the dependence of lifetimes on geomagnetic activity is different from the dayside. It is clearly seen that lifetimes for $Kp = 0.75$ in Figure 2e are shorter than those for $Kp = 3$ in Figure 2f. This is due to the fact that for $Kp \geq 1.8$, the hiss intensity strongly decreases at latitudes larger than 15° (Figures 1k and 1l), and for small $Kp < 1.8$, the waves extend to $|\lambda| \geq 15°$ (Figure 1j).

The computed lifetimes are sensitive to radial distance. Both on the dayside and nightside, the lifetimes of electrons with energies from 1 keV to tens of keV decrease with increasing distance from a hundred days to several days and hours. The lifetimes of hundreds of keV electrons strongly decrease from $L = 3$ to $L \sim 3.5$–4.5 and then slightly increase with increasing distance to $L = 6$. For relativistic energies $E_k > 1$ MeV, the lifetimes tend to increase with increasing L shell.

Lifetimes also exhibit a strong dependence on energy on both dayside and nightside. With increasing energy from 1 keV, the lifetimes tend to decrease from hundreds of days to several days or less, depending on geomagnetic activity, with a local minimum at hundreds of keV at small L shells to tens of keV at larger distances. The lifetimes of electrons with relativistic energies strongly increase with increasing energy. For example, during active geomagnetic conditions $Kp = 6$ at $L = 3.5$, the lifetimes of 0.5 MeV and 3 MeV electrons are 18 h and 10 days, respectively, on the dayside.

3.3. Parameterization of Lifetimes

Next, we perform analytical parameterizations of lifetimes that can be easily incorporated into convection and particle tracing codes to account for the pitch angle scattering of energetic electrons by hiss waves.

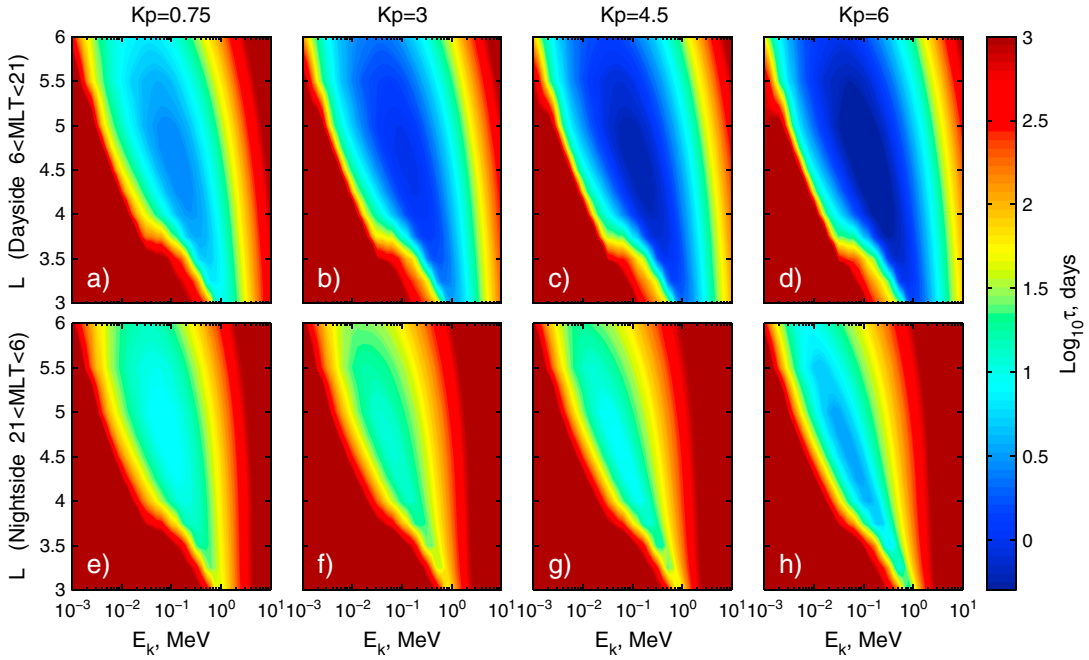

Figure 2. Electron lifetimes, τ, in days for (a–d) the dayside and (e–h) nightside as a function of L and kinetic energy for four values of Kp.

Since nightside lifetimes contribute very little to the total lifetimes, we only provide parameterization of lifetimes for the dayside in the main text. Parameterizations for the nightside lifetimes are presented in the supporting information. We also provide the tabulated computed lifetimes for both sectors in the supporting information.

Parameterized lifetimes for the 6–21 MLT sector are given by

$$\log_{10}\tau = g(E,L) + y(Kp), \tag{6}$$

where $L = 3$–6, $E = \log_{10}(E_k)$ for $E_k = 1$ keV–10 MeV taken in MeV units, and $Kp \le 6$. Function $g(E, L)$ represents $\log_{10}\tau$ for $Kp = 6$ and is given by

$$\begin{aligned} g(E,L) = {} & a_1 + a_2L + a_3E + a_4L^2 + a_5LE + a_6E^2 + a_7L^3 + a_8L^2E + a_9LE^2 + a_{10}E^3 + a_{11}L^4 + a_{12}L^3E + a_{13}L^2E^2 \\ & + a_{14}LE^3 + a_{15}E^4 + a_{16}L^4E + a_{17}L^3E^2 + a_{18}L^2E^3 + a_{19}LE^4 + a_{20}E^5 + a_{21}L^3E^3 + a_{22}L^2E^4 + a_{23}LE^5 \\ & + a_{24}E^6 + a_{25}L^3E^4 + a_{26}L^2E^5 + a_{27}LE^6 + a_{28}E^7, \end{aligned} \tag{7}$$

and

$$y(Kp) = 0.015465Kp^2 - 0.26074Kp + 1.0077. \tag{8}$$

We first used linear regression method to fit the logarithm of lifetime for $Kp = 6$. Since for high geomagnetic activity, lifetimes larger than 100 days are not physically interesting; we only parameterized lifetimes starting from energies for which lifetimes become less than 100 days for $Kp = 6$ (or following equation (8) less than 1000 days for $Kp = 0$). Therefore, the obtained parameterization (equation (7)) is only valid for $E > f(L)$, where

$$f(L) = -0.2573L^4 + 4.2781L^3 - 25.9348L^2 + 66.8113L - 66.1182. \tag{9}$$

The expression in equation (7) has polynomials of E and L up to seventh order including interaction terms. This high order was chosen for parameterization to accurately model the lowest lifetimes. The coefficients for parameterization in equation (7) are presented in the supporting information. The coefficient of determination for the $g(E, L)$ parameterization at $Kp = 6$ is 0.987. The accuracy is calculated as $A = (\tau_c - \tau_p)/\tau_c \cdot 100\%$, where τ_c and τ_p are the computed and parameterized lifetimes, respectively. The mean of absolute accuracy for $g(E, L)$ parameterization for $E > f(L)$ is 14%. Our results showed that the activity dependence is very similar for all considered values of L and E. To determine the dependence on Kp, we determined the functional

dependence (equation (8)) for various values of L and E. Our results showed that the coefficients in this dependence vary by approximately 10^{-4}% and thus can simply use a functional dependence $y(Kp)$ that is independent of the radial distance and energy.

3.4. Comparison of Lifetimes With Previous Observations

Next, we compare the computed lifetimes with those from some previous observational studies. Lifetimes are usually estimated from observations by analyzing the exponential decay of fluxes at certain range of equatorial pitch angles. *Baker et al*. [1994] analyzed the decay rate of relativistic electrons $E_k > 400$ keV at distances $2.5 \le L \le 5$ using SAMPEX data and found that lifetimes were approximately 5 to 10 days. Our computed lifetimes for low geomagnetic activity are quantitatively similar with the results of *Baker et al*. [1994].

Meredith et al. [2006b] explored the loss time scales of electrons using CRRES observations during low geomagnetic activity ($Kp < 3$) following enhanced geomagnetic activity. The results of *Meredith et al*. [2006b] showed that at distances from 3 to 5 Earth's radii, the lifetimes of electrons with energies 214 keV, 510 keV, and 1.09 MeV lie in the range of 1.5–3.5, 2.5–5.5, and 5.5–6.5 days, respectively, where larger values of lifetimes correspond to larger L shells. Similar observational results were obtained by *Benck et al*. [2010]. They estimated the lifetimes of electrons using SAC-C and DEMETER low-altitude measurements after high geomagnetic activity when *Dst* index fell below −50 nT. The lifetimes obtained by *Benck et al*. [2010] for 0.16–1.36 MeV electrons lied in the range of 3 to 8 days at $L = 3$–4.8. The observed lifetimes by *Meredith et al*. [2006b] and *Benck et al*. [2010] are consistent with our model results for quiet and moderate geomagnetic activities, except for energies ~150–400 keV at $3 \le L < 3.6$, where the computed lifetimes become significantly larger with decreasing distance reaching the values of tens or hundred days.

4. Summary and Discussions

Hiss waves play an important role in the loss of the inner magnetosphere electrons. In this study, we derived a database of hiss observations from the CRRES spacecraft using a technique nearly identical to that of *Meredith et al*. [2004]. We used regression analysis to develop simple quadratic fits to the data as a function of Kp, L, and λ for two different local time sectors. Coefficients for the model are provided.

We also theoretically examine the effect of hiss waves on the decay rates of electrons. Hiss wave intensity dependencies obtained in this work are used to calculate electron lifetimes in the 6–21 and 21–6 MLT sectors. We use a realistic wave normal angle distribution, which is dependent on latitude, and take into account the increase of plasma density with increasing latitude. We find that lifetimes are highly dependent on radial distance, electron kinetic energy, and value of Kp index. Hiss waves can scatter electrons at certain energies and distances within several days during quiet geomagnetic activity and within less than a day during the disturbed conditions. The comparison of the computed lifetimes with observational studies shows a good agreement except for electrons of ~150–400 keV energies at $3 < L < 3.6$. At these distances and energies, the diffusion coefficients due to hiss waves have deep local minimum at equatorial pitch angles around 60°–80°, and therefore, following equation (2), the obtained lifetimes have large values. Interaction of electrons with magnetosonic waves [e.g., *Shprits et al*., 2013a, 2013b] can fill this gap in the scattering rates at $L \ge 3$ and thus cause the decrease of lifetimes. Scattering of hundreds of keV electrons by lightning-generated whistlers can also reduce the lifetime values at distances less than 3.6 Earth's radii [e.g., *Abel and Thorne*, 1998]. It should be also noted that the measured decay rates can be actually influenced by the local acceleration and radial transports. Improvements of the hiss wave models using multiple satellite measurements in the future may also partially resolve the discrepancy between the observed and computed lifetimes.

The lifetimes on the dayside are parameterized (equation (6)) for use in various convection and particle tracing codes. The obtained parameterizations are only valid for L shells from 3 to 6, Kp indices less than 6, and electron energies $\log_{10}(E_k) > f(L)$ in the range from 1 keV to 10 MeV, where $f(L)$ is determined in equation (10). We showed that lifetimes have a nonlinear dependence on geomagnetic activity (equation (8)). We also give parameterizations of lifetimes on the nightside and provide the tabulated computed lifetimes for both sectors in the supporting information. It should be noted that both the hiss intensity model and parameterizations of electron lifetimes can be only used within the plasmasphere, which can be strongly compressed up to several Earth's radii during active geomagnetic conditions.

Acknowledgments

The *Kp* index was provided by the Kyoto World Data Center. The CRRES ephemeris data were provided by the Satellite Situation Center Web. Table 1 and the supporting information contain data supporting Figures 1 and 2. All data used in this study can be accessed through the sources listed above or by contacting the authors. Authors would like to thank Nigel Meredith and Margaret Chen for useful discussions. The research of K. Orlova was supported by the NASA Living with a Star Jack Eddy Postdoctoral Fellowship Program, administered by the University Corporation for Atmospheric Research. The work of M. Spasojevic was supported by AFRL award FA9453-11-C-0011. This research was also supported by the UC-Lab Fee program, NASA grants NNX10AK99G and NNX13AE34G, and NSF AGS-1203747.

The Editor thanks Thomas O'Brien and an anonymous reviewer for their assistance in evaluating this paper.

References

Abel, B., and R. M. Thorne (1998), Electron scattering loss in Earth's inner magnetosphere 1 Dominant physical processes, *J. Geophys. Res.*, *103*, 2385–2396, doi:10.1029/97JA02919.

Agapitov, O., A. Artemyev, V. Krasnoselskikh, Y. V. Khotyaintsev, D. Mourenas, H. Breuillard, M. Balikhin, and G. Rolland (2013), Statistics of whistler-mode waves in the outer radiation belt: Cluster STAFF-SA measurements, *J. Geophys. Res. Space Physics*, *118*, 3407–3420, doi:10.1002/jgra.50312.

Albert, J. M. (2000), Pitch-angle diffusion as seen by CRRES, *Adv. Space Res.*, *25*, 2343–2346.

Albert, J. M., and Y. Y. Shprits (2009), Estimates of lifetimes against pitch angle diffusion, *J. Atmos. Sol. Terr. Phys.*, *71*, 1647–1652, doi:10.1016/j.jastp.2008.07.004.

Anderson, R., D. Gurnett, and D. Odem (1992), CRRES plasma wave experiment, *J. Spacecr. Rockets*, *29*(4), 570.

Artemyev, A. V., D. Mourenas, O. V. Agapitov, and V. V. Krasnoselskikh (2013), Parametric validations of analytical lifetime estimates for radiation belt electron diffusion by whistler waves, *Ann. Geophys.*, *31*, 599–624, doi:10.5194/angeo-31-599-2013.

Baker, D. N., J. B. Blake, L. B. Callis, J. R. Cummings, D. Hovestadt, S. Kanekal, B. Klecker, R. A. Mewaldt, and R. D. Zwickl (1994), Relativistic electron acceleration and decay time scales in the inner and outer radiation belts: Sampex, *Geophys. Res. Lett.*, *21*(6), 409–412, doi:10.1029/93GL03532.

Benck, S., L. Mazzino, M. Cyamukungu, M. J. Cabrera, and V. Pierrard (2010), Low altitude energetic electron lifetimes after enhanced magnetic activity as deduced from SAC-C and DEMETER data, *Ann. Geophys.*, *28*, 849–859, doi:10.5194/angeo-28-849-2010.

Bortnik, J., R. M. Thorne, and N. P. Meredith (2008), The unexpected origin of plasmaspheric hiss from discrete chorus emissions, *Nature*, *452*, 62, doi:10.1038/nature06741.

Chen, M. W., and M. Schulz (2001), Simulations of diffuse aurora with plasma sheet electrons in pitch angle diffusion less than everywhere strong, *J. Geophys. Res.*, *106*(A12), 28,949–28,966, doi:10.1029/2001JA000138.

Denton, R. E., J. D. Menietti, J. Goldstein, S. L. Young, and R. R. Anderson (2004), Electron density in the magnetosphere, *J. Geophys. Res.*, *109*, A09215, doi:10.1029/2003JA010245.

Denton, R. E., K. Takahashi, I. A. Galkin, P. A. Nsumei, X. Huang, B. W. Reinisch, R. R. Anderson, M. K. Sleeper, and W. J. Hughes (2006), Distribution of density along magnetospheric field lines, *J. Geophys. Res.*, *111*, A04213, doi:10.1029/2005JA011414.

Glauert, S. A., and R. B. Horne (2005), Calculation of pitch angle and energy diffusion coefficients with the PADIE code, *J. Geophys. Res.*, *110*, A04206, doi:10.1029/2004JA010851.

Lam, M. M., R. B. Horne, N. P. Meredith, and S. A. Glauert (2009), Radiation belt electron flux variability during three CIR-driven geomagnetic storms, *J. Atmos. Sol. Terr. Phys.*, *71*, 1145, doi:10.1016/j.jastp.2008.06.007.

Ledocq, M. J., D. A. Gurnett, and R. R. Anderson (1994), Electron number density fluctuations near the plasmapause observed by the CRRES spacecraft, *J. Geophys. Res.*, *99*(A12), 23,661–23,671, doi:10.1029/94JA02294.

Lyons, L. R., and R. M. Thorne (1973), Equilibrium structure of radiation belt electrons, *J. Geophys. Res.*, *78*(13), 2142–2149, doi:10.1029/JA078i013p02142.

Lyons, L. R., R. M. Thorne, and C. F. Kennel (1972), Pitch-angle diffusion of radiation belt electrons within the plasmasphere, *J. Geophys. Res.*, *77*(19), 3455–3474, doi:10.1029/JA077i019p03455.

Meredith, N. P., R. B. Horne, R. M. Thorne, D. Summers, and R. R. Anderson (2004), Substorm dependence of plasmaspheric hiss, *J. Geophys. Res.*, *109*, A06209, doi:10.1029/2004JA010387.

Meredith, N. P., R. B. Horne, M. A. Clilverd, D. Horsfall, R. M. Thorne, and R. R. Anderson (2006a), Origins of plasmaspheric hiss, *J. Geophys. Res.*, *111*, A09217, doi:10.1029/2006JA011707.

Meredith, N. P., R. B. Horne, S. A. Glauert, R. M. Thorne, D. Summers, J. M. Albert, and R. R. Anderson (2006b), Energetic outer zone electron loss timescales during low geomagnetic activity, *J. Geophys. Res.*, *111*, A05212, doi:10.1029/2005JA011516.

Meredith, N. P., R. B. Horne, S. A. Glauert, and R. R. Anderson (2007), Slot region electron loss timescales due to plasmaspheric hiss and lightning-generated whistlers, *J. Geophys. Res.*, *112*, A08214, doi:10.1029/2007JA012413.

Meredith, N. P., R. B. Horne, S. A. Glauert, D. N. Baker, S. G. Kanekal, and J. M. Albert (2009), Relativistic electron loss timescales in the slot region, *J. Geophys. Res.*, *114*, A03222, doi:10.1029/2008JA013889.

Millan, R. M., and R. M. Thorne (2007), Review of radiation belt relativistic electron loss, *J. Atmos. Sol. Terr. Phys.*, *69*, 362–377, doi:10.1016/j.jastp.2006.06.019.

Moldwin, M. B., L. Downward, H. K. Rassoul, R. Amin, and R. R. Anderson (2002), A new model of the location of the plasmapause: CRRES results, *J. Geophys. Res.*, *107*(A11), 1339, doi:10.1029/2001JA009211.

Mourenas, D., and J.-F. Ripoll (2012), Analytical estimates of quasi-linear diffusion coefficients and electron lifetimes in the inner radiation belt, *J. Geophys. Res.*, *117*, A01204, doi:10.1029/2011JA016985.

Selesnick, R. S., J. B. Blake, and R. A. Mewaldt (2003), Atmospheric losses of radiation belt electrons, *J. Geophys. Res.*, *108*(A12), 1468, doi:10.1029/2003JA010160.

Shprits, Y. Y., D. A. Subbotin, N. P. Meredith, and S. R. Elkington (2008), Review of modeling of losses and sources of relativistic electrons in the outer radiation belt II: Local acceleration and loss, *J. Atmos. Sol. Terr. Phys.*, *70*, 1694–1713.

Shprits, Y. Y., D. Subbotin, and B. Ni (2009), Evolution of electron fluxes in the outer radiation belt computed with the VERB code, *J. Geophys. Res.*, *114*, A11209, doi:10.1029/2008JA013784.

Shprits, Y. Y., A. Runov, and B. Ni (2013a), Gyro-resonant scattering of radiation belt electrons during the solar minimum by fast magnetosonic waves, *J. Geophys. Res. Space Physics*, *118*, 648–652, doi:10.1002/jgra.50108.

Shprits, Y. Y., D. Subbotin, A. Drozdov, M. E. Usanova, A. Kellerman, K. Orlova, D. N. Baker, D. L. Turner, and K.-C. Kim (2013b), Unusual stable trapping of the ultra-relativistic electrons in the Van Allen Radiation Belts, *Nat. Phys.*, *9*, 699–703, doi:10.1038/nphys2760.

Summers, D., B. Ni, N. P. Meredith, R. B. Horne, R. M. Thorne, M. B. Moldwin, and R. R. Anderson (2008), Electron scattering by whistler-mode ELF hiss in plasmaspheric plumes, *J. Geophys. Res.*, *113*, A04219, doi:10.1029/2007JA012678.

Thorne, R. M., et al. (2013), Evolution and slow decay of an unusual narrow ring of relativistic electrons near L ~ 3.2 following the September 2012 magnetic storm, *Geophys. Res. Lett.*, *40*, 3507–3511, doi:10.1002/grl.50627.